

# Direct observations of wave-sea ice interactions in the Antarctic Marginal Ice Zone

Stina Wahlgren<sup>1</sup>, Jim Thomson<sup>2</sup>, Louise C. Biddle<sup>1</sup>, and Sebastiaan Swart<sup>1</sup>

<sup>1</sup>University of Gothenburg

<sup>2</sup>University of Washington

April 20, 2023

## Abstract

Wave energy propagating into the Antarctic marginal ice zone affects the quality and extent of the sea ice, and wave propagation is therefore an important factor for understanding and predicting changes in sea ice cover. Sea ice is notoriously hard to model and in-situ observations of wave activity in the Antarctic marginal ice zone are scarce, due to the extreme conditions of the region. Here, we provide new in-situ data from two drifting Surface Wave Instrument Float with Tracking (SWIFT) buoys deployed in the Weddell Sea in the austral winter and spring in 2019. The buoy location ranges from open water to more than 200 km into the sea ice. We estimate the attenuation of swell with wave periods 8-18 s, and find an attenuation coefficient  $a = 4 \cdot 10^{-6}$  to  $7 \cdot 10^{-5} \text{ m}^{-1}$  in spring, and approximately five-fold larger in winter. The attenuation coefficients show a power law frequency dependence, with power coefficient 3.3 in spring and 4 in winter. The in-situ data also shows a change in wave direction, where wave direction tends to be more perpendicular to the ice edge farther into the sea ice. A possible explanation for this might be a change in the dispersion relation caused by changing sea ice composition. These observations can help shed further light on the influence of sea ice on waves propagating into the Marginal Ice Zone, aiding development of coupled wave-sea ice models.

1 **Direct observations of wave-sea ice interactions in the**  
2 **Antarctic Marginal Ice Zone**

3 **S. Wahlgren<sup>1</sup>, J. Thomson<sup>2</sup>, L. C. Biddle<sup>1,3</sup>, S. Swart<sup>1</sup>**

4 <sup>1</sup>Department of Marine Sciences, University of Gothenburg, Gothenburg, Sweden

5 <sup>2</sup>Applied Physics Laboratory, University of Washington, Seattle, Washington

6 <sup>3</sup>Voice of the Ocean, Gothenburg, Sweden

7 **Key Points:**

- 8 • SWIFT buoy data show that frequency dependence of wave attenuation in sea ice  
9 follows a power law, with exponent 3-4.  
10 • Both wave attenuation and the frequency dependence of attenuation were stronger  
11 in winter than in spring.  
12 • Observations suggest a change in wave direction as a function of distance from the  
13 sea ice edge.

---

Corresponding author: Stina Wahlgren, [stina.wahlgren@gu.se](mailto:stina.wahlgren@gu.se)

## Abstract

Wave energy propagating into the Antarctic marginal ice zone affects the quality and extent of the sea ice, and wave propagation is therefore an important factor for understanding and predicting changes in sea ice cover. Sea ice is notoriously hard to model and in-situ observations of wave activity in the Antarctic marginal ice zone are scarce, due to the extreme conditions of the region. Here, we provide new in-situ data from two drifting Surface Wave Instrument Float with Tracking (SWIFT) buoys deployed in the Weddell Sea in the austral winter and spring in 2019. The buoy location ranges from open water to more than 200 km into the sea ice. We estimate the attenuation of swell with wave periods 8-18 s, and find an attenuation coefficient  $\alpha = 4 \cdot 10^{-6}$  to  $7 \cdot 10^{-5} \text{ m}^{-1}$  in spring, and approximately five-fold larger in winter. The attenuation coefficients show a power law frequency dependence, with power coefficient 3.3 in spring and 4 in winter. The in-situ data also shows a change in wave direction, where wave direction tends to be more perpendicular to the ice edge farther into the sea ice. A possible explanation for this might be a change in the dispersion relation caused by changing sea ice composition. These observations can help shed further light on the influence of sea ice on waves propagating into the Marginal Ice Zone, aiding development of coupled wave-sea ice models.

## Plain Language Summary

Changes in the sea ice extent around Antarctica affects the global climate, and it is therefore important to accurately represent sea ice in climate models. One feature that is generally missing in climate models is the interaction between ocean waves and sea ice. Ocean waves change the sea ice, for example by breaking up ice floes into smaller ones. At the same time, the sea ice reduces the strength of the waves so that the wave height decreases and eventually disappears far into the sea ice. How far into the sea ice waves reach depends both on the size of the waves and on the sea ice. Due to the complexity of sea ice, theoretical models of how waves and sea ice interact are still in development. In order to better represent the wave-sea ice interactions in climate models, simple but accurate models of how fast sea ice reduces the strength of waves is needed. Using two wave buoys, we measured the wave activity in the Antarctic sea ice during two expeditions in 2019. Together with similar measurements from other parts of the Antarctic sea ice, this can help to improve predictions of sea ice cover.

## 1 Introduction

The sea ice around Antarctica is important for global climate in several ways. Loss of Antarctic sea ice has been linked to ice shelf disintegration, by allowing storm-induced swell waves to reach exposed ice shelf fronts, leading to accelerating loss of the Antarctic ice sheet and increase in sea level rise (Massom et al., 2018). The growth and melt of sea ice acts as a freshwater sink/source, and ocean-atmosphere interactions, such as exchange of heat or momentum, are also affected by the ice condition (Vichi et al., 2019). The transition between the open ocean and permanent sea ice is called the Marginal Ice Zone (MIZ). Multiple definitions of the MIZ exist, depending on purpose and field of study it can be defined based on wave activity as a region where waves and sea ice co-exist (Montiel et al., 2022), based on seasonal ice growth and melt or simply as the region between 15% and 80% sea ice concentration. In the Antarctic the width of this zone can be hundreds of kilometres (Toffoli et al., 2015).

One factor that influences the MIZ and its sea ice condition is surface gravity waves. Waves affect ice formation (Shen & Ackley, 1991/ed) and can break big ice floes into smaller ones (Langhorne et al., 1998/ed), altering dynamical properties and heat exchange. One key property determining to what extent this happens is the significant wave height (Toffoli et al., 2015). In return, the MIZ also affects surface waves by attenuating them, thus in-

64 fluencing how far into the ice the waves reach and can affect the sea ice. Incorporating  
65 coupled sea ice-wave models into climate models is therefore important for improving  
66 predictions of for example MIZ extent and distribution. Yet, wave-ice coupling is still  
67 generally neglected in polar climate modelling (Kousal et al., 2022). Lack of observations  
68 also leaves weak constraints on models (Cooper et al., 2022), meaning that future pre-  
69 dictions and current parameterizations have large uncertainties.

70 It is well established that the amplitude of waves decreases with distance travelled  
71 in ice, and that the sea ice acts as a low-pass filter, attenuating higher frequency waves  
72 more rapidly than waves with lower frequencies. The exact nature of the attenuation,  
73 and how much of it that can be attributed to energy dissipation versus scattering, has  
74 long been debated (Squire, 2018)(Thomson, 2022), but recent observations point to dis-  
75 sipation as an important factor (Ardhuin et al., 2020)(Voermans et al., 2019). Waves trav-  
76 elling into the MIZ are typically thought to decay exponentially, which was first reported  
77 in (Wadhams et al., 1988) based on several field experiments in the Arctic MIZ. Since  
78 then, many studies have reproduced this result. There are some observations of linear  
79 decay for long wavelengths and high significant wave height (Montiel et al., 2018)(Meylan  
80 et al., 2014), which might reflect non-linear phenomena or be artefacts due to small data  
81 sets and different ice conditions (Kohout et al., 2020). Many studies have shown a so-  
82 called “roll over” effect, where attenuation is not decreasing with increasing frequency  
83 for all frequencies. This roll-over effect has recently been explained in (Thomson et al.,  
84 2021) as an artefact due to frequency dependent modulation noise, introduced in data  
85 collection and signal processing. Wind-generated waves in sea ice could also have con-  
86 tributed to the observed roll-over effect (Li et al., 2017).

87 The frequency dependence of the attenuation is typically modelled as a power law  
88 dependence, or as a sum of power laws. Different physical processes are expected to re-  
89 sult in different frequency dependence. Observations from both the Arctic and the Antarc-  
90 tic MIZ consistently shows a power coefficient between 2 and 4 (Meylan et al., 2018), af-  
91 fected by physical parameters such as sea ice type and concentration, floe size and wave  
92 period (Montiel et al., 2022) (Kohout et al., 2020)(Meylan et al., 2018). W. E. Rogers  
93 et al. (2021), found a strong positive correlation between attenuation and sea ice thick-  
94 ness. Further, Ardhuin et al. (2020) emphasise that attenuation mechanisms differ vastly  
95 between the outer break-up region, where waves cause the sea ice to form floes, and the  
96 inner region with continuous ice sheets. Wind direction can also influence attenuation,  
97 where head-wind has been observed to increase attenuation (Montiel et al., 2022).

98 Observations of frequency dependence attenuation in the Antarctic MIZ are scarce.  
99 Meylan et al. (2014) described the attenuation coefficient for wave periods 2-20 s as a  
100 sum of two power laws of order 2 and 4, based on data from an array of 5 wave buoys  
101 deployed in September 2012 during the SIPEX-II campaign. The most extensive wave  
102 buoy data set is from the PIPERS expedition, where 14 buoys were deployed in the Ross  
103 Sea, collecting data between April and July 2017 (Kohout et al., 2020). Neither of these  
104 wave buoys provide wave direction. W. E. Rogers et al. (2021) used a subset of the PIPERS  
105 data set, collected in June 2017. Montiel et al. (2022) found a power coefficient 2.5 based  
106 on another subset of the PIPERS data set collected in April-May 2017.

107 In this study we present new wave buoy data from the Weddell Sea. We use this  
108 to derive frequency dependent attenuation in the Antarctic MIZ for both austral win-  
109 ter and spring. We also show a correlation between wave direction and distance to the  
110 ice edge that might be attributed to a change in the dispersion relation.

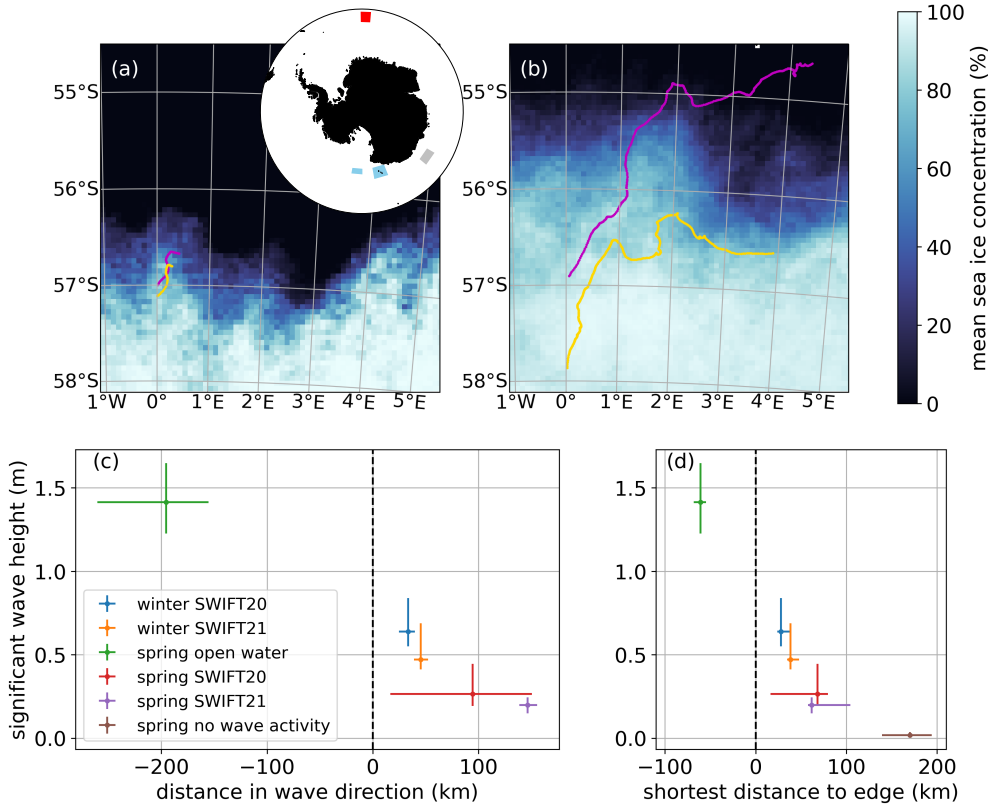


**Figure 1.** Overview of the two SWIFT deployments. Average sea ice concentration over the time span the buoys were deployed, together with tracks for SWIFT20 (magenta) and SWIFT21 (yellow), during a) winter deployment and b) spring deployment. Inset: Geographic location of the SWIFT deployments (red), together with the locations of the PIPERS data set (light blue) (Kohout et al., 2020) and SIPEX II data set (grey) (Meylan et al., 2014). c) Median and quartiles of significant wave height for all four deployments as a function of distance to ice edge in the energy-weighted wave direction, as measured by the buoy. The SWIFT20 spring deployment is split into in-ice ( $SIC \geq 15\%$ ) and open water ( $SIC < 15\%$ ). d) Same as c, but as a function of the shortest distance to the ice edge. Data with no measurable wave activity ( $H_s < 0.1\text{m}$ ) is shown in a separate category.

## 2 Materials and Methods

### 2.1 SWIFT Buoy and Deployments

We use data from two SWIFT v3 buoys (Thomson, 2012) deployed in the MIZ in the Southern Ocean as part of the ROAM-MIZ project ([www.roammiz.com](http://www.roammiz.com)) during the SCALE research voyages in 2019. The buoys were equipped with GPS logger, inertial measurement units (IMU), meteorological stations (airmar WX-200 Ultrasonic weather stations) and a low resolution camera. The two buoys, here referred to as SWIFT20 and SWIFT21, were deployed in austral winter (July 27-28) and austral spring (October 23 – November 7). They recorded a total of 17 days of data (16 days simultaneously with both buoys) with different ice types and weather conditions. SWIFT buoys are deployed directly into the water, and measure wave periods in the range 2-20 s, corresponding to wavelengths 6-600 m in deep open water. This covers all but the highest frequencies of the wind-wave interactions.

In winter, SWIFT20 was deployed at 57°S, 0°E, approximately 25 km into the sea ice pack. SWIFT21 was deployed approximately 10 km south of SWIFT20, further into the sea ice field, and they stayed approximately 10 km apart while drifting north (Figure 1a). The sea ice consisted of 1-5 m pancakes, around 40 cm thick, with WMO (code 3739) ice age ID3 (predominantly new and/or young ice with some first-year ice) (Skatulla et al., 2022). Photos of the ice taken from the ship are provided by (de Vos et al., 2019). The edge of the MIZ was further south in the winter than during the spring deployment, and was advancing north during and after the winter deployment.

For the two week long spring deployment, SWIFT20 was deployed at the same site as the winter deployment, which was then around 100 km from the ice edge. The sea ice consisted of 1-5 m ice floes with slush in between. SWIFT21 was deployed around 100 km south of SWIFT20 (Figure 1b), in the ship track in densely packed, consolidated ice floes. Again, both buoys drifted north. After approximately 9 days, SWIFT20 drifted out of the ice into open water, while SWIFT21 stayed in the sea ice during the deployment. On recovery of SWIFT21, the sea ice consisted of 1-5 m ice floes with water present between the ice floes. Photos from deployment and recovery are presented in the supplementary material (Figure S1-S3).

### 2.2 Wave spectrum

SWIFT buoys estimate the wave field by measuring the horizontal (GPS) and vertical (IMU) displacement of the buoy. The power spectral density,  $E(f)$ , is derived from the displacements by assuming a circular orbital motion (Thomson et al., 2018), which is predicted by linear wave theory for waves in deep open water. The validity of this assumption is measured with the check factor, which is simply the ratio between the measured horizontal and vertical displacement (Thomson et al., 2015). This ratio should be equal to 1, and large deviations from this indicates that the measurement is not reliable.

Significant wave height,  $H_s$ , is computed from the wave spectrum with

$$H_s = 4 \cdot \sqrt{\int E(f) df}, \quad (1)$$

Data with  $H_s < 0.1$  m is not used in further analysis due to low signal-to-noise ratio (SNR).

In addition to the 1D wave spectrum, SWIFT buoys provide the standard directional moments of the spectrum ( $a_1, b_1, a_2, b_2$ ). The dominant direction for each frequency bin can be derived from the cross correlation of the displacements (both horizontal and vertical) using the first directional moments  $a_1$  and  $b_1$  (see the appendix in Thomson et al. (2018) for details). We define the mean wave direction,  $\Theta$ , for a frequency band lim-

157 ited by  $f_1, f_2$  as the energy weighted dominant direction

$$\Theta = \arctan(\bar{b}_1, \bar{a}_1), \quad (2)$$

158 where

$$\bar{a}_1 = \frac{\int_{f_1}^{f_2} E(f) a_1(f) df}{\int_{f_1}^{f_2} E(f) df} \quad (3)$$

159 is the energy weighted directional moment. The spread of the mean direction,  $\Delta\Theta$ , is  
160 computed as

$$\Delta\Theta = \sqrt{2 \left( 1 - \sqrt{\bar{a}_1^2 + \bar{b}_1^2} \right)}. \quad (4)$$

### 161 2.3 Defining the ice edge

162 In order to determine the distance travelled by waves in sea ice, we need to esti-  
163 mate the location of the transition between open water and the MIZ, here called the sea  
164 ice edge. We estimate the ice edge based on AMSR-E sea ice concentration (SIC). The  
165 dataset had a spatial resolution of 6.25 x 6.25 km and provided daily (Melsheimer & Spreen,  
166 2019). The sea ice concentration was interpolated to hourly resolution in order to match  
167 the SWIFT data. The AMSR-E sea ice concentration was compared to SAR images (GRD,  
168 HH-band) from Sentinel-1 (0.1 x 0.1 km, 6 day resolution) when available in our study  
169 region. Sea ice concentration and SAR images showed good agreement compared to the  
170 sea ice extent (Figure 2a).

171 The ice edge was detected from sea ice concentration as follows: for each time in-  
172 stance, a binary map was created, with zeros where sea ice concentration was less than  
173 15 % and ones where sea ice concentration was 15 % or more. The binary map was then  
174 smoothed using a 2D Gaussian filter with a standard deviation  $\sigma_{\text{edge}}$  of 1 pixel (6.25 km),  
175 and the ice edge was defined as the 0.5 contour line of the smoothed map. An example  
176 of sea ice concentration and derived ice edge is shown in Figure 2b.

177 The ice edge was roughly aligned in the east-west direction, but was observed to  
178 be very dynamic in its orientation and location. During the spring deployment, the ice  
179 edge shifted more than 100 km north during the first 6 days, illustrating that the Antarc-  
180 tic MIZ is prone to large spatial changes over short periods (Figure 2c).

### 181 2.4 Local ice condition

182 In addition to co-located AMSR-E sea ice concentration data, imagery from cam-  
183 eras mounted on the masts of the SWIFT buoys were used to categorise the local ice con-  
184 dition (Figure 3). The cameras were approximately 1 m above the surface, and captured  
185 one photo every 4 seconds for the first 8 minutes of every hour. The images were anal-  
186 ysed manually. Photos captured during the dark hours (around 8pm - 4am local time  
187 for the Spring deployment), as well as blurry photos were discarded. The blurriness of-  
188 ten occurred during morning hours and typically disappeared after a couple of hours, prob-  
189 ably due to ice on the lens. Time lapses of the imagery are provided in the supplemen-  
190 tary materials (Movie S1-S3).

191 Due to limitations of the imagery, existing established ice scales, such as the Antarc-  
192 tic Sea Ice Processes and Climate (ASPeCT) protocol were not applicable. The main lim-  
193 itations are a limited field of view and no available size reference (except for a few feath-  
194 ery friends - Figure 3), which makes it hard to determine ice thickness and floe size. An  
195 ice type scale designed specifically for SWIFT imagery was introduced in W. Rogers et  
196 al. (2018) (Hošeková et al., 2020), but this only covers pancake ice. We therefore devel-  
197 oped a new ice scale (Table 1). The scale is inspired by the ASPeCT protocol and uses

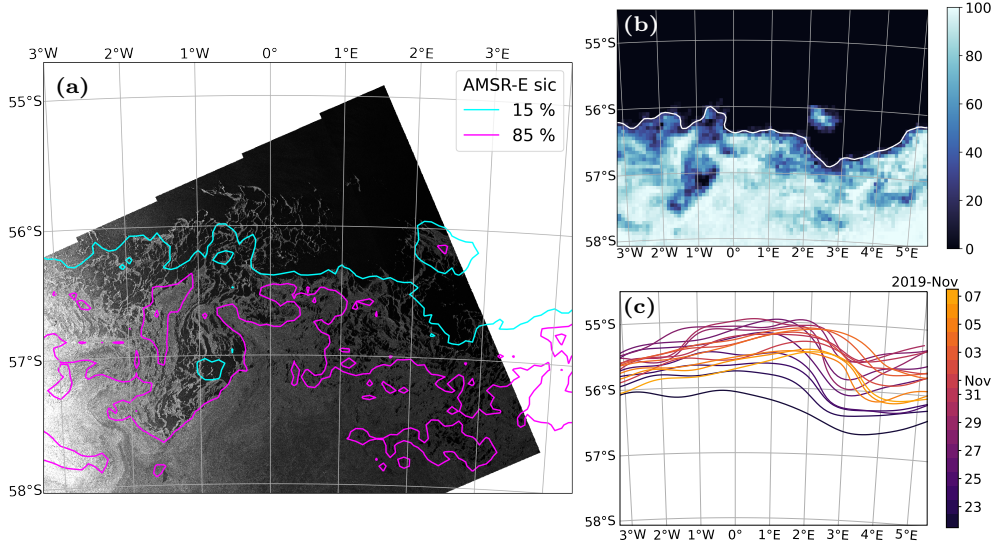


**Figure 2.** Locating the ice edge from AMSR-E sea ice concentration. a) Comparison between sea ice concentration and Sentinel-1 SAR imagery. b) Example of ice edge (white) derived from AMSR-E sea ice concentration. c) The movement of the ice edge during the spring deployment. For illustration purposes, a smoother version of the edge ( $\sigma_{\text{edge}} = 37.5 \text{ km}$ ) is shown.

**Table 1.** Ice scale used for quantifying local ice condition based on SWIFT buoy on-board imagery.

Ice Code	Description
-1	Open water patch deep in sea ice
1	Open water
2	Open water and trace ice
3	Small pancakes (<1m)
4	Brash
5	Ice cakes/floes with frazil or open water
6	Ice cakes/floes with brash
7	Tightly packed ice cakes/floes

198 terminology as defined in World Meteorological Organisation (WMO) Sea-Ice Nomen-  
 199 clature. Example imagery is shown in Figure 3. Based on the imagery, each hour was  
 200 assigned an ice code (Figure 4).

## 201 **2.5 Distance to the edge**

202 The peak wave direction measured with SWIFT was generally towards south east,  
 203 indicating an oblique incidence from the ice edge. We use two different measures of distance  
 204 to the ice edge: the shortest distance to the edge and the distance in respect to  
 205 the wave direction. The latter one is the one that matters for wave attenuation, but it  
 206 is also sensitive to errors in estimated wave direction. For determining wave direction,  
 207 the energy-weighted mean wave direction was used, as defined in equation 2 at the buoy

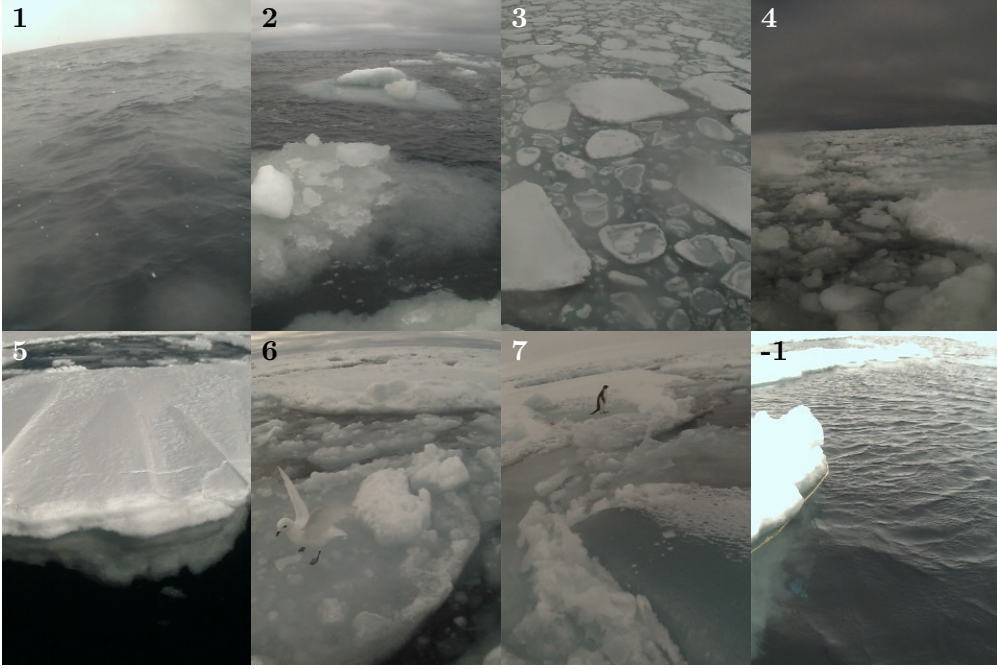


**Figure 3.** Examples of SWIFT on-board imagery and ice codes.

208 location. Distance in wave direction was not computed for data points with  $H_s < 0.1$  m,  
 209 since no reliable wave direction could be derived for those points.

210 Distance was determined in AMSR sea ice concentration coordinates. This is a po-  
 211 lar stereographic projection, referenced at  $70^\circ\text{S}$ ,  $0^\circ$  (Melsheimer, 2019), thus giving a dis-  
 212 tortion of 11-12% at the buoy location. Compared to other uncertainties, this is small  
 213 and therefore not accounted for.

## 214 **2.6 Wave attenuation**

215 We derive spectral wave attenuation assuming exponential decay with distance:

$$E(d, f) = E_0(f)e^{-\alpha(f)d}, \quad (5)$$

216 where  $\alpha(f)$  is the (frequency dependent) attenuation coefficient,  $E_0(f)$  the power spec-  
 217 tral density at a reference point and  $E(f)$  is the power spectral density after attenua-  
 218 tion by sea ice during a distance  $d$ . There is an implicit assumption that the attenua-  
 219 tion coefficient does not change over the distance  $d$ .

220 We only use data where we have data from both buoys and where both buoys recorded  
 221 a significant wave height of at least 0.1 m. During the spring deployment, SWIFT21 was  
 222 deep in sea ice and did not record almost any wave activity for the first part of the de-  
 223 ployment (Figure 4). We therefore only use data from 2019-10-31 to 2019-11-08, where  
 224 SWIFT21 generally observed wave activity and SWIFT20 was in open water. The check  
 225 factor was generally  $\ll 1$  when  $E(f) < 10^{-4}$   $\text{m}^2/\text{Hz}$ , which was true for most part of  
 226 the spectrum in sea ice (Figure 4). We attribute this to wave attenuation below the in-  
 227 strument noise level, and therefore only focus on the frequency band  $0.05 \leq f \leq 0.13$  Hz  
 228 for this study. In total, this filtering resulted in 36 data point pairs in winter and 100  
 229 data point pairs in spring, for each of the seven analysed frequency bins.

230 For each pair of data points, the attenuation coefficient was defined as

$$\alpha(f) = \frac{\ln(E_{\text{SWIFT20}}(f)) - \ln(E_{\text{SWIFT21}}(f))}{d} \quad (6)$$

231 where the power spectral density measurement by SWIFT20 was used as the reference  
 232 value. In winter, both buoys were in the ice, and we defined  $d$  as the effective separa-  
 233 tion between the both buoys along the incident wave direction. For each time stamp, we  
 234 defined the incident wave direction as the average of the energy weighted wave direction  
 235 between the two buoys. In spring, SWIFT20 was in open water, and  $d$  was then defined  
 236 as the distance from SWIFT21 to the ice edge in the energy weighted wave direction as  
 237 measured in sea ice by SWIFT21.

238 We did not account for the time it would take for waves to travel the effective sep-  
 239 aration between SWIFT20 and SWIFT21. For the analysed frequency band, this cor-  
 240 responds to a time delay of 2-5 hours per 100 km based on the dispersion relation for  
 241 linear waves in deep water. In winter, the buoys were so close that this time lag is shorter  
 242 than the time resolution. Even though the time lag in spring is large, the temporal vari-  
 243 ation in spectral energy density is small compared to the difference between buoys. The  
 244 effect of the time delay on the estimated attenuation coefficient is therefore expected to  
 245 be small compared to other uncertainties.

### 246 3 Result and discussion

247 The significant wave height measured by the buoys were around 0.5-1 m during the  
 248 winter deployment. In spring, SWIFT20 generally measured significant wave heights around  
 249 0.2 m while in ice, with two notable events where the significant wave height increased  
 250 to almost 1 m (Figure 4). While in open water, SWIFT20 measured significant wave heights  
 251 between 1.5 – 3 m. SWIFT21 was arguably not in the MIZ during the first 9 days as al-  
 252 most no wave activity was recorded (Figure 4).

253 The maximum observed wave height was 2.7 m in open water (SWIFT20, Novem-  
 254 ber 17) and 1.7 m in ice (SWIFT20, October 23). No significant wave activity was ob-  
 255 served more than 200 km from the ice edge in wave direction (150 km from ice edge clos-  
 256 est direction) (Figure 5b). Wave activity was observed in 100 % sea ice concentration  
 257 (Figure 4), illustrating that waves can reach beyond the sea ice concentration-based def-  
 258 inition of the MIZ.

259 The measured wave spectra and significant wave height illustrates some of the key  
 260 effects sea ice has on surface waves. In the ice, the significant wave height is typically  
 261 much lower (Figure 1c-d), and the high frequency content diminishes (Figure 4c,f). One  
 262 notable event is the transition from sea ice to open water by SWIFT20 around 31 Oc-  
 263 tober. This event is seen as a step increase in significant wave height as well as an in-  
 264 crease in higher frequency content of several orders of magnitude, and is confirmed by  
 265 SWIFT on-board imagery (Figure 4a-c). It coincides fairly well with the co-located sea  
 266 ice concentration. Between 2-4 November, when SWIFT20 is in open water, there are  
 267 three instances where the high frequency content drops. The first one occurred during  
 268 the dark hours, thus lacking on-board imagery, but for the other two on-board imagery  
 269 confirms that this is due to sea ice.

#### 270 3.1 Spectral wave attenuation

271 Box-and-whisker plots of the observed attenuation coefficients is shown in Figure  
 272 5, together with non-linear least square fits to the power law

$$\alpha(f) = af^b \quad (7)$$

273 The fitted parameters are presented in Table 2. A clear trend with increasing attenu-  
 274 ation for increasing frequencies is seen. No roll over effect is observed, which indicates

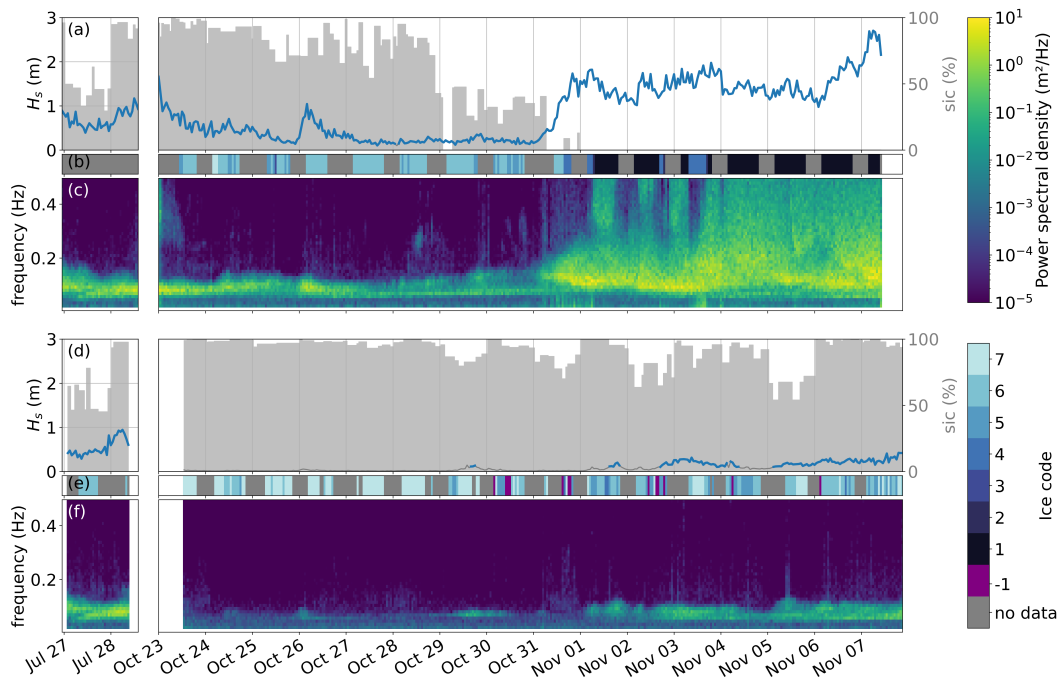


**Figure 4.** Overview of the data collected by SWIFT20 (top) and SWIFT21 (bottom) in winter (left panels) and spring (right panels). (a,d) Significant wave height (blue line) and wave spectra measured by SWIFT, together with co-located sea ice concentration (shaded grey) from AMSR-E. Significant wave height of less than 0.1 m is shown in grey. (b,e) Local ice condition based on SWIFT on-board imagery. (c,f) Spectral power density.

**Table 2.** Parameter estimates for the power law  $\alpha = af^b$ , using non-linear least squares.

deployment	$a$	$b$	constraint
spring	0.065	3.3	none
winter	8.4	4.9	none
winter	1.3	4.0	$2 \leq b \leq 4$

275 that the data filtering process described in section 2.6 was successful in avoiding spu-  
 276 rious negative biases from instrument noise.

277 Attenuation rates for both spring and winter are in the order of magnitudes  $10^{-5}$ –  
 278  $10^{-4} \text{ m}^{-1}$ . The attenuation coefficient is roughly 5 times larger in winter than spring,  
 279 but both the winter and spring observations are consistent with previous observations  
 280 in the Antarctic MIZ (Figure 6). SWIFT on-board imagery and ship observations show  
 281 that the buoys were clearly in the break-up region (or open water) during the part of  
 282 the deployments used for deriving wave attenuation.

283 No significant attenuation is seen for the lowest frequency bins in winter (Figure  
 284 5). Since the distance between buoys were around 10 km, an attenuation coefficient  $\alpha$   
 285 of  $10^{-5} \text{ m}^{-1}$  would result in a difference of power density spectrum of only 10%, which  
 286 is probably too low to measure given the circumstances.

287 The frequency dependence of the attenuation rate is consistent with power law for  
 288 both data sets (Figure 5). In spring, the fitted power coefficient  $b = 3.3$  is consistent  
 289 with the constraint  $2 \leq b \leq 4$  suggested in (Meylan et al., 2018). In winter, the curve  
 290 fit gave  $b = 4.9$ , higher than the predictions by Meylan et al, but adding a constraint  
 291  $2 \leq b \leq 4$  results in a very similar fit (Figure 5a). Since no measurable attenuation is  
 292 seen for the lower frequency bins in winter, fitting a two parameter model to this data  
 293 set is prone to overfitting. It is clear that  $b$  lies in the higher region of those predicted  
 294 by Meylan et al, but too much weight should not be put on the exact value.

295 The ice condition during the winter deployment was similar for the whole data set  
 296 in the area around the buoys. Thanks to extensive ice observations from the ship, (Skatulla  
 297 et al., 2022), (de Vos et al., 2019), the ice condition is well described.

298 In contrast to the winter deployment, the attenuation should be seen as an inte-  
 299 grated effect over a wide range of ice conditions (covering all from the transition from  
 300 open water to more than 100 km into the MIZ). Even so, it is worth noting that the spring  
 301 deployment is much deeper into the MIZ and in higher sea ice concentration, while ex-  
 302 perencing a much lower attenuation rate.

### 303 3.2 Change in wave direction

304 Figure 7a shows the energy weighted wave direction of the swell band  $0.05 \leq f \leq$   
 305  $0.13 \text{ Hz}$  for the spring deployment as a function of distance to the ice edge. The clus-  
 306 ter of points 2019-10-24 to 2019-10-27 is collected by SWIFT20 and associated with a  
 307 rapid northward movement of the ice edge (Figure 2c) and two wave events (Figure 4a).  
 308 We therefore believe that this cluster belongs to another wave field, not representative  
 309 for the rest of the deployment. Apart from this cluster, a clear trend is seen, where the  
 310 wave direction tends to be more towards the south, and thus more perpendicular to the  
 311 ice edge, with increasing distance travelled in sea ice.

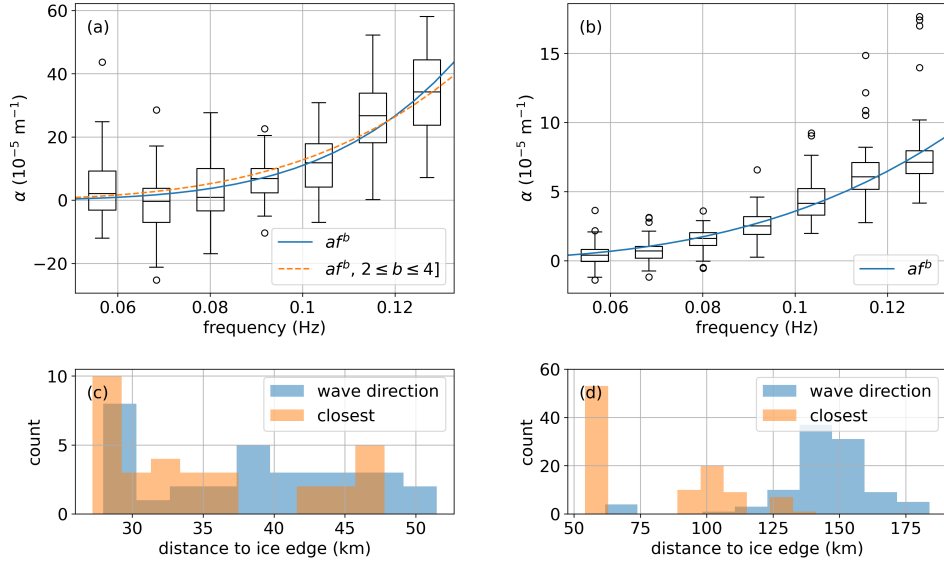


**Figure 5.** (top) Box-and-whisker plots of the attenuation rates as a function of wave frequency, together with power law-fits. The fitted parameters are presented in Table 2. a) Data from the winter deployment, where the distance in wave direction between the buoys was around 16 km. Each frequency bin has 36 data points. b) Data from the spring deployment, where one buoy was in open water and the other in sea ice. Each frequency bin has 100 data points. (bottom) Histogram of the distance to the ice edge for the two data sets in (c) winter (mean of the two buoys) and (d) spring.

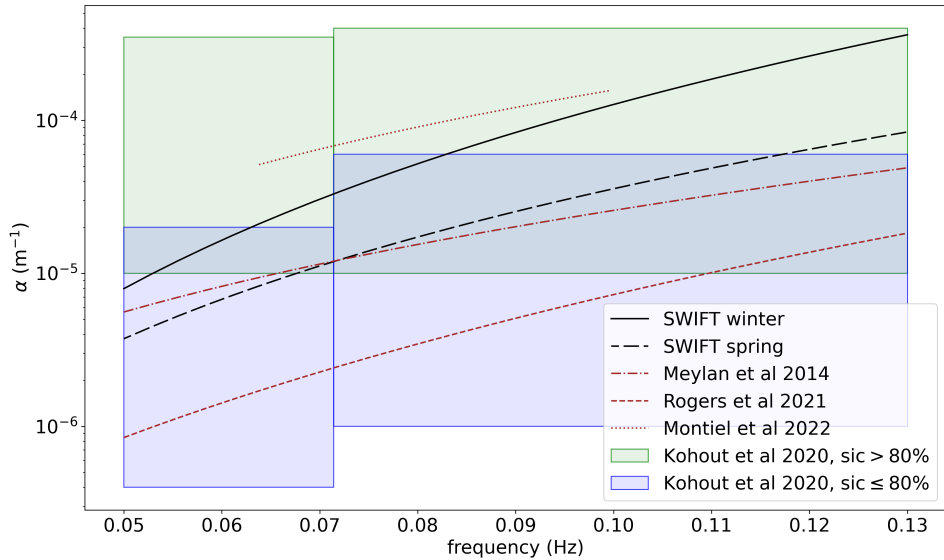


**Figure 6.** Comparison with other observations of spectral wave attenuation in the Antarctic MIZ: Attenuation based on the SIPEX-II data set in September 2012 Meylan et al. (2014) and various derivations from the large PIPERS data set presented by Kohout et al. (2020). W. E. Rogers et al. (2021) used the eastern subset of this data set, collected in June 2017, while the western subset, collected in April-May 2017, was used by Montiel et al. (2022).

312 In order to further study this effect, we binned the data into 50 km-groups based  
 313 on the closest distance to the ice edge. Data points before 2019-10-28 were excluded from  
 314 analysis based on the reasoning above. The change in wave direction coincides with an  
 315 increase in sea ice concentration and a decrease in directional spread (Figure 7b-d).

316 A strong correlation between distance to ice edge and wave direction is observed.  
 317 Since the two buoys drifted towards the ice edge during the deployment, distance to the  
 318 ice edge and time is highly correlated in this data set. Therefore, the finding should ac-  
 319 count for this. Still, the same trend is seen where we have simultaneous measurements  
 320 for both buoys (Figure 7a). Since in-situ measurements of wave direction in the Antarc-  
 321 tic MIZ is rare, (the most extensive data sets are from WIIOS buoys, which does not pro-  
 322 vide direction measurements), we find these results valuable enough to report. A sim-  
 323 ilar observation has been made from Sentinel-1 SAR data in the Barents Sea (Monteban  
 324 et al., 2019). We see two plausible mechanisms that could cause wave direction to shift  
 325 towards normal with increasing distance from the ice edge: an actual change in wave di-  
 326 rection due to refraction, or an apparent change in wave direction due to wave attenu-  
 327 ation (spatial filtering).

328 If the observed change in wave direction is caused by refraction, it would mean that  
 329 the waves slow down (group speed decreases) as they propagate through the sea ice. It  
 330 is important to point out that refraction happens due to changes in the dispersion re-  
 331 lation. This is distinct from wave attenuation, which does not require a change in the  
 332 medium (on the contrary, it is typically assumed a constant attenuation in order to be  
 333 able to quantify it from observations). In order for refraction to explain the continuous  
 334 change in dominant wave direction observed in the data, there must therefore be a con-  
 335 tinuous change in the dispersion relation, where waves progressively slow down as they  
 336 travel further into the ice. Figure 7c shows a change in co-located sea ice concentration  
 337 that matches the observed change in wave direction. Note that at these scales, the sea  
 338 ice concentration may be seen as a proxy for the overall ice condition. We know from  
 339 the SWIFT onboard imagery that the sea ice quality changes drastically between mea-  
 340 surements close to the ice edge and far into the sea ice.

341 Actual surface waves will always have a spread in direction, i.e. the waves do not  
 342 have exactly the same direction. This means that even if the open water wave field was  
 343 entirely homogeneous, the waves reaching a certain point in the sea ice would come from  
 344 different directions, and thus have travelled different distances in the sea ice. This means  
 345 that the waves with a more oblique incidence angle would have travelled farther, and there-  
 346 fore would be more attenuated, shifting the dominant direction towards normal while  
 347 decreasing the directional spread. We do observe some decrease in directional spread with  
 348 increasing distance from the ice edge (Figure 7c), but further analysis is required to de-  
 349 termine if this decrease is enough to explain the change in direction.

## 350 4 Summary

351 Two wave buoys were deployed in the Atlantic Antarctic MIZ during the SCALE  
 352 cruises in austral winter and spring in 2019 to observe wave-sea ice interactions. No wave  
 353 activity was observed more than 200 km into the MIZ, while the open water wave field  
 354 had a significant wave height around 2-3 m in spring.

355 From this data set, we have derived spectral wave attenuation coefficients for wave  
 356 frequencies between 0.05 and 0.13 Hz. The attenuation coefficients were around  $4 \cdot 10^{-6}$   
 357 to  $7 \cdot 10^{-5} \text{ m}^{-1}$  in spring, and approximately five-fold larger in winter. This is in agree-  
 358 ment with in-situ studies of the Pacific Antarctic MIZ. The frequency dependent is con-  
 359 sistent with a power law dependency, with a power coefficient of around 4 in winter and  
 360 3.3 in spring.

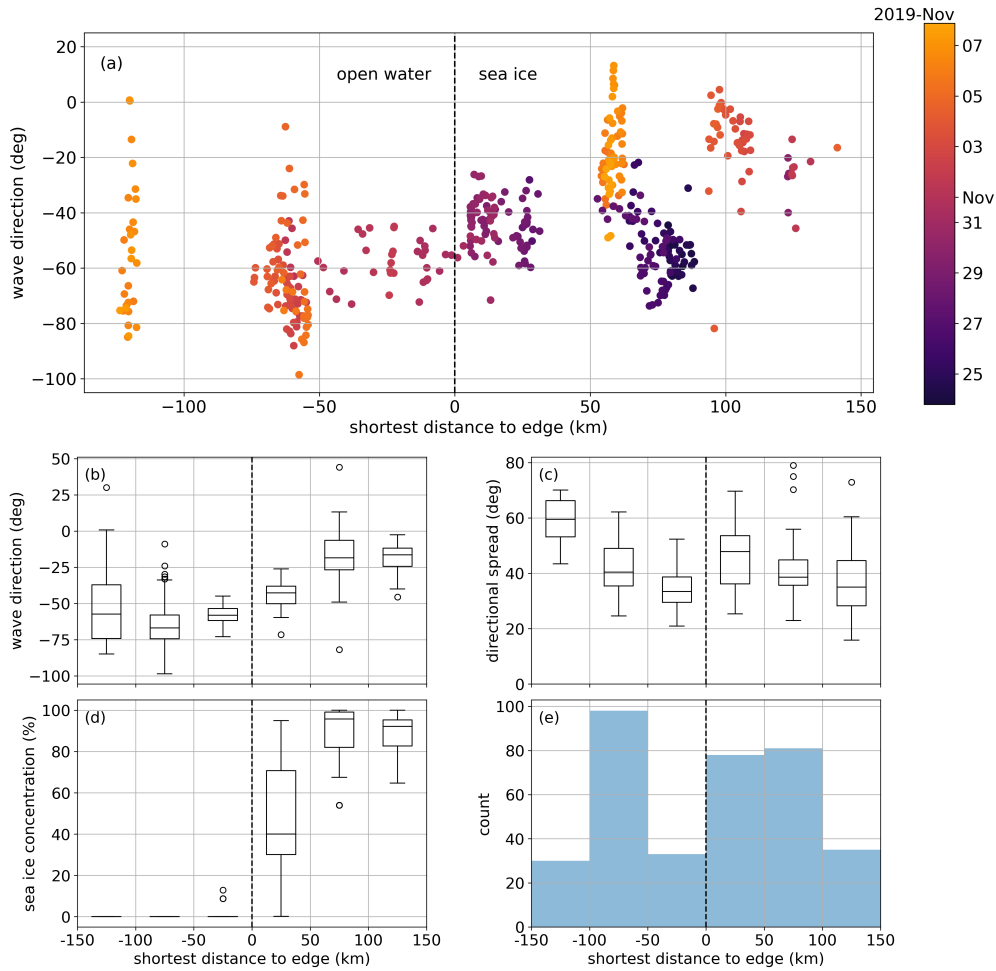


**Figure 7.** Energy weighted wave direction of the swell band  $0.05 \leq f \leq 0.13$  as a function of distance to the ice edge, measured by SWIFT buoys during the spring deployment. (a) Scatter plot of all measurements, coloured by time. (b-d) Box-and-whisker plots of (b) wave direction, (c) directional spread and (d) co-located sea ice concentration, collected after 2019-10-27, binned by distance to the ice edge. The number of data points per bin is shown in (e).

361 A relationship between wave direction and distance to ice edge was observed in the  
 362 data, where the wave direction tends to be more perpendicular to the ice edge deeper  
 363 in sea ice. This could be a sign of refraction, where the propagation velocity changes with  
 364 sea ice condition.

### 365 Acknowledgments

366 This work was supported by the following grants of S. Swart: Wallenberg Academy Fel-  
 367 lowship (WAF 2015.0186), Swedish Research Council (VR 2019-04400), STINT-NRF Mo-  
 368 bility Grant (STINT180910357293). S. Swart has received funding from the European  
 369 Union's Horizon 2020 research and innovation program under Grant agreement no. 821001  
 370 (SO-CHIC). L.C Biddle's time was supported by the VR grant 2020-04281. Alex de Klerk  
 371 and Joe Talbert built and prepared the SWIFT buoys. The authors thank Sea Technol-  
 372 ogy Services (STS), SANAP, the Captain, and crew of the S.A. Agulhas II for their field-  
 373 work/technical assistance. The authors also thank Isabelle Giddy, Hanna Rosenthal, Jo-  
 374 han M. Edholm, Kevin Thielen and all other participants of the SCALE cruises who helped  
 375 with deployment, spotting and recovery of the SWIFT buoys.

### 376 Data Availability Statement

377 The sea-ice data is made available via <https://seaice.uni-bremen.de/databrowser/>.  
 378 Sentinel-1 SAR imagery is available via <https://dataspace.copernicus.eu/browser/>.  
 379 The code used for this analysis is available at [https://github.com/stinawahlgren/](https://github.com/stinawahlgren/roammiz-wave-seaice-interactions)  
 380 [roammiz-wave-seaice-interactions](https://github.com/stinawahlgren/roammiz-wave-seaice-interactions) and SWIFT buoy data is available at [https://](https://doi.org/10.5281/zenodo.7845764)  
 381 [doi.org/10.5281/zenodo.7845764](https://doi.org/10.5281/zenodo.7845764). SWIFT buoy data has been processed using [https://](https://github.com/SASlabgroup/SWIFT-codes)  
 382 [github.com/SASlabgroup/SWIFT-codes](https://github.com/SASlabgroup/SWIFT-codes).

### 383 References

- 384 Ardhuin, F., Otero, M., Merrifield, S., Grouazel, A., & Terrill, E. (2020). Ice  
 385 Breakup Controls Dissipation of Wind Waves Across Southern Ocean Sea  
 386 Ice. *Geophysical Research Letters*, *47*(13), e2020GL087699. Retrieved from  
 387 <https://onlinelibrary.wiley.com/doi/abs/10.1029/2020GL087699> doi:  
 388 10.1029/2020GL087699
- 389 Cooper, V. T., Roach, L. A., Thomson, J., Brenner, S. D., Smith, M. M., Meylan,  
 390 M. H., & Bitz, C. M. (2022, September). Wind waves in sea ice of the western  
 391 Arctic and a global coupled wave-ice model. *Philosophical Transactions of the*  
 392 *Royal Society A: Mathematical, Physical and Engineering Sciences*, *380*(2235),  
 393 20210258. Retrieved from [https://royalsocietypublishing.org/doi/](https://royalsocietypublishing.org/doi/10.1098/rsta.2021.0258)  
 394 [10.1098/rsta.2021.0258](https://royalsocietypublishing.org/doi/10.1098/rsta.2021.0258) doi: 10.1098/rsta.2021.0258
- 395 de Vos, M., Ramjukadh, C.-L., Liesker, C. G., de Villiers, M., & Lyttle, C. T.  
 396 (2019, September). *Southern Ocean Marginal Ice Zone Photographs from*  
 397 *a 2019 Winter Research Cruise (SA Agulhas II)*. PANGAEA. Re-  
 398 trieved from <https://doi.pangaea.de/10.1594/PANGAEA.905497> doi:  
 399 10.1594/PANGAEA.905497
- 400 Hošeková, L., Malila, M. P., Rogers, W. E., Roach, L. A., Eidam, E., Rainville,  
 401 L., ... Thomson, J. (2020). Attenuation of Ocean Surface Waves in Pan-  
 402 cake and Frazil Sea Ice Along the Coast of the Chukchi Sea. *Journal of*  
 403 *Geophysical Research: Oceans*, *125*(12), e2020JC016746. Retrieved from  
 404 <https://onlinelibrary.wiley.com/doi/abs/10.1029/2020JC016746> doi:  
 405 10.1029/2020JC016746
- 406 Kohout, A. L., Smith, M., Roach, L. A., Williams, G., Montiel, F., & Williams,  
 407 M. J. M. (2020, September). Observations of exponential wave attenuation in  
 408 Antarctic sea ice during the PIPERS campaign. *Annals of Glaciology*, *61*(82),  
 409 196–209. Retrieved from <https://www.cambridge.org/core/journals/>

- annals-of-glaciology/article/observations-of-exponential-wave  
-attenuation-in-antarctic-sea-ice-during-the-pipers-campaign/  
A21809218DA23F5DE46CC0D823922A55 doi: 10.1017/aog.2020.36
- 410  
411  
412  
413 Kousal, J., Voermans, J. J., Liu, Q., Heil, P., & Babanin, A. V. (2022). A Two-  
414 Part Model for Wave-Sea Ice Interaction: Attenuation and Break-Up. *Journal*  
415 *of Geophysical Research: Oceans*, 127(5), e2022JC018571. Retrieved from  
416 <https://onlinelibrary.wiley.com/doi/abs/10.1029/2022JC018571> doi:  
417 10.1029/2022JC018571
- 418 Langhorne, P. J., Squire, V. A., Fox, C., & Haskell, T. G. (1998/ed). Break-  
419 up of sea ice by ocean waves. *Annals of Glaciology*, 27, 438–442. Re-  
420 trieved from [https://www.cambridge.org/core/journals/annals](https://www.cambridge.org/core/journals/annals-of-glaciology/article/breakup-of-sea-ice-by-ocean-waves/DCDE1C3D4F33A59B8EE12DC940DB0F61)  
421 [-of-glaciology/article/breakup-of-sea-ice-by-ocean-waves/](https://www.cambridge.org/core/journals/annals-of-glaciology/article/breakup-of-sea-ice-by-ocean-waves/DCDE1C3D4F33A59B8EE12DC940DB0F61)  
422 [DCDE1C3D4F33A59B8EE12DC940DB0F61](https://www.cambridge.org/core/journals/annals-of-glaciology/article/breakup-of-sea-ice-by-ocean-waves/DCDE1C3D4F33A59B8EE12DC940DB0F61) doi: 10.3189/S0260305500017869
- 423 Li, J., Kohout, A. L., Doble, M. J., Wadhams, P., Guan, C., & Shen, H. H.  
424 (2017). Rollover of Apparent Wave Attenuation in Ice Covered Seas. *Jour-*  
425 *nal of Geophysical Research: Oceans*, 122(11), 8557–8566. Retrieved from  
426 <https://onlinelibrary.wiley.com/doi/abs/10.1002/2017JC012978> doi:  
427 10.1002/2017JC012978
- 428 Massom, R. A., Scambos, T. A., Bennetts, L. G., Reid, P., Squire, V. A., & Stam-  
429 merjohn, S. E. (2018, June). Antarctic ice shelf disintegration triggered  
430 by sea ice loss and ocean swell. *Nature*, 558(7710), 383–389. Retrieved  
431 from <https://www.nature.com/articles/s41586-018-0212-1> doi:  
432 10.1038/s41586-018-0212-1
- 433 Melsheimer, C. (2019). *ASI Version 5 Sea Ice Concentration User Guide*.
- 434 Melsheimer, C., & Spreen, G. (2019, February). *AMSR2 ASI sea ice concentration*  
435 *data, Antarctic, version 5.4 (NetCDF) (July 2012 - December 2019)*. PAN-  
436 GAEA. Retrieved from <https://doi.pangaea.de/10.1594/PANGAEA.898400>  
437 doi: 10.1594/PANGAEA.898400
- 438 Meylan, M. H., Bennetts, L. G., & Kohout, A. L. (2014). In situ measure-  
439 ments and analysis of ocean waves in the Antarctic marginal ice zone. *Geo-*  
440 *physical Research Letters*, 41(14), 5046–5051. Retrieved from [https://](https://onlinelibrary.wiley.com/doi/abs/10.1002/2014GL060809)  
441 [onlinelibrary.wiley.com/doi/abs/10.1002/2014GL060809](https://onlinelibrary.wiley.com/doi/abs/10.1002/2014GL060809) doi:  
442 10.1002/2014GL060809
- 443 Meylan, M. H., Bennetts, L. G., Mosig, J. E. M., Rogers, W. E., Doble, M. J., &  
444 Peter, M. A. (2018). Dispersion Relations, Power Laws, and Energy Loss for  
445 Waves in the Marginal Ice Zone. *Journal of Geophysical Research: Oceans*,  
446 123(5), 3322–3335. Retrieved from [https://onlinelibrary.wiley.com/doi/](https://onlinelibrary.wiley.com/doi/abs/10.1002/2018JC013776)  
447 [abs/10.1002/2018JC013776](https://onlinelibrary.wiley.com/doi/abs/10.1002/2018JC013776) doi: 10.1002/2018JC013776
- 448 Monteban, D., Lubbad, R., & Johnsen, H. (2019). Sentinel-1 sar observa-  
449 tions of peak wavelength and dominant wave direction in the marginal  
450 ice zone of the barents sea. *Proceedings - International Conference on*  
451 *Port and Ocean Engineering under Arctic Conditions*. Retrieved from  
452 <https://ntnuopen.ntnu.no/ntnu-xmlui/handle/11250/2639926>
- 453 Montiel, F., Kohout, A. L., & Roach, L. A. (2022, May). Physical Drivers of Ocean  
454 Wave Attenuation in the Marginal Ice Zone. *Journal of Physical Oceanogra-*  
455 *phy*, 52(5), 889–906. Retrieved from [https://journals.ametsoc.org/view/](https://journals.ametsoc.org/view/journals/phoc/52/5/JPO-D-21-0240.1.xml)  
456 [journals/phoc/52/5/JPO-D-21-0240.1.xml](https://journals.ametsoc.org/view/journals/phoc/52/5/JPO-D-21-0240.1.xml) doi: 10.1175/JPO-D-21-0240.1
- 457 Montiel, F., Squire, V. A., Doble, M., Thomson, J., & Wadhams, P. (2018). Attenu-  
458 ation and Directional Spreading of Ocean Waves During a Storm Event in the  
459 Autumn Beaufort Sea Marginal Ice Zone. *Journal of Geophysical Research:*  
460 *Oceans*, 123(8), 5912–5932. Retrieved from [https://onlinelibrary.wiley](https://onlinelibrary.wiley.com/doi/abs/10.1029/2018JC013763)  
461 [.com/doi/abs/10.1029/2018JC013763](https://onlinelibrary.wiley.com/doi/abs/10.1029/2018JC013763) doi: 10.1029/2018JC013763
- 462 Rogers, W., Posey, P., Li, L., & Allard, R. (2018, April). Forecasting and Hindcast-  
463 ing Waves In and Near the Marginal Ice Zone: Wave Modeling and the ONR  
464 Sea State Field Experiment.. Retrieved from <https://www.semanticscholar>

- 465 .org/paper/Forecasting-and-Hindcasting-Waves-In-and-Near-the  
 466 -Rogers-Posey/5583f6d20c399b17bbebd4efc347c0bb0b69a01a
- 467 Rogers, W. E., Meylan, M. H., & Kohout, A. L. (2021, February). Estimates of  
 468 spectral wave attenuation in Antarctic sea ice, using model/data inversion.  
 469 *Cold Regions Science and Technology*, 182, 103198. Retrieved from [https://](https://www.sciencedirect.com/science/article/pii/S0165232X20304456)  
 470 [www.sciencedirect.com/science/article/pii/S0165232X20304456](https://www.sciencedirect.com/science/article/pii/S0165232X20304456) doi:  
 471 10.1016/j.coldregions.2020.103198
- 472 Shen, H. H., & Ackley, S. F. (1991/ed). A one-dimensional model for wave-  
 473 induced ice-floe collisions. *Annals of Glaciology*, 15, 87–95. Retrieved from  
 474 [https://www.cambridge.org/core/journals/annals-of-glaciology/](https://www.cambridge.org/core/journals/annals-of-glaciology/article/onedimensional-model-for-waveinduced-icefloe-collisions/32F3295E93860E65517AE0310F8033C7)  
 475 [article/onedimensional-model-for-waveinduced-icefloe-collisions/](https://www.cambridge.org/core/journals/annals-of-glaciology/article/onedimensional-model-for-waveinduced-icefloe-collisions/32F3295E93860E65517AE0310F8033C7)  
 476 [32F3295E93860E65517AE0310F8033C7](https://www.cambridge.org/core/journals/annals-of-glaciology/article/onedimensional-model-for-waveinduced-icefloe-collisions/32F3295E93860E65517AE0310F8033C7) doi: 10.3189/1991AoG15-1-87-95
- 477 Skatulla, S., Audh, R. R., Cook, A., Hepworth, E., Johnson, S., Lupascu, D. C., ...  
 478 Vichi, M. (2022, July). Physical and mechanical properties of winter first-  
 479 year ice in the Antarctic marginal ice zone along the Good Hope Line. *The*  
 480 *Cryosphere*, 16(7), 2899–2925. Retrieved from [https://tc.copernicus.org/](https://tc.copernicus.org/articles/16/2899/2022/)  
 481 [articles/16/2899/2022/](https://tc.copernicus.org/articles/16/2899/2022/) doi: 10.5194/tc-16-2899-2022
- 482 Squire, V. A. (2018, August). A fresh look at how ocean waves and sea ice inter-  
 483 act. *Philosophical Transactions of the Royal Society A: Mathematical, Physi-*  
 484 *cal and Engineering Sciences*, 376(2129), 20170342. Retrieved from [https://](https://royalsocietypublishing.org/doi/full/10.1098/rsta.2017.0342)  
 485 [royalsocietypublishing.org/doi/full/10.1098/rsta.2017.0342](https://royalsocietypublishing.org/doi/full/10.1098/rsta.2017.0342) doi: 10  
 486 .1098/rsta.2017.0342
- 487 Thomson, J. (2012, December). Wave Breaking Dissipation Observed with “SWIFT”  
 488 Drifters. *Journal of Atmospheric and Oceanic Technology*, 29(12), 1866–1882.  
 489 Retrieved from [https://journals.ametsoc.org/view/journals/atot/29/](https://journals.ametsoc.org/view/journals/atot/29/12/jtech-d-12-00018.1.xml)  
 490 [12/jtech-d-12-00018.1.xml](https://journals.ametsoc.org/view/journals/atot/29/12/jtech-d-12-00018.1.xml) doi: 10.1175/JTECH-D-12-00018.1
- 491 Thomson, J. (2022, September). Wave propagation in the marginal ice zone:  
 492 Connections and feedback mechanisms within the air–ice–ocean system.  
 493 *Philosophical Transactions of the Royal Society A: Mathematical, Physi-*  
 494 *cal and Engineering Sciences*, 380(2235), 20210251. Retrieved from  
 495 <https://royalsocietypublishing.org/doi/10.1098/rsta.2021.0251>  
 496 doi: 10.1098/rsta.2021.0251
- 497 Thomson, J., Girton, J. B., Jha, R., & Trapani, A. (2018, February). Measurements  
 498 of Directional Wave Spectra and Wind Stress from a Wave Glider Autonomous  
 499 Surface Vehicle. *Journal of Atmospheric and Oceanic Technology*, 35(2), 347–  
 500 363. Retrieved from [https://journals.ametsoc.org/view/journals/atot/](https://journals.ametsoc.org/view/journals/atot/35/2/jtech-d-17-0091.1.xml)  
 501 [35/2/jtech-d-17-0091.1.xml](https://journals.ametsoc.org/view/journals/atot/35/2/jtech-d-17-0091.1.xml) doi: 10.1175/JTECH-D-17-0091.1
- 502 Thomson, J., Hošeková, L., Meylan, M. H., Kohout, A. L., & Kumar, N. (2021).  
 503 Spurious Rollover of Wave Attenuation Rates in Sea Ice Caused by Noise  
 504 in Field Measurements. *Journal of Geophysical Research: Oceans*, 126(3),  
 505 e2020JC016606. Retrieved from [https://onlinelibrary.wiley.com/doi/](https://onlinelibrary.wiley.com/doi/abs/10.1029/2020JC016606)  
 506 [abs/10.1029/2020JC016606](https://onlinelibrary.wiley.com/doi/abs/10.1029/2020JC016606) doi: 10.1029/2020JC016606
- 507 Thomson, J., Talbert, J., de Klerk, A., Brown, A., Schwendeman, M., Gold-  
 508 smith, J., ... Meinig, C. (2015, June). Biofouling Effects on the Response  
 509 of a Wave Measurement Buoy in Deep Water. *Journal of Atmospheric*  
 510 *and Oceanic Technology*, 32(6), 1281–1286. Retrieved from [https://](https://journals.ametsoc.org/view/journals/atot/32/6/jtech-d-15-0029.1.xml)  
 511 [journals.ametsoc.org/view/journals/atot/32/6/jtech-d-15-0029.1.xml](https://journals.ametsoc.org/view/journals/atot/32/6/jtech-d-15-0029.1.xml)  
 512 doi: 10.1175/JTECH-D-15-0029.1
- 513 Toffoli, A., Bennetts, L. G., Meylan, M. H., Cavaliere, C., Alberello, A., Elsnab,  
 514 J., & Monty, J. P. (2015). Sea ice floes dissipate the energy of steep ocean  
 515 waves. *Geophysical Research Letters*, 42(20), 8547–8554. Retrieved from  
 516 <https://onlinelibrary.wiley.com/doi/abs/10.1002/2015GL065937> doi:  
 517 10.1002/2015GL065937
- 518 Vichi, M., Eayrs, C., Alberello, A., Bekker, A., Bennetts, L., Holland, D., ... Tof-  
 519 foli, A. (2019). Effects of an Explosive Polar Cyclone Crossing the Antarctic

- 520 Marginal Ice Zone. *Geophysical Research Letters*, 46(11), 5948–5958. Retrieved  
521 from <https://onlinelibrary.wiley.com/doi/abs/10.1029/2019GL082457>  
522 doi: 10.1029/2019GL082457
- 523 Voermans, J. J., Babanin, A. V., Thomson, J., Smith, M. M., & Shen, H. H. (2019).  
524 Wave Attenuation by Sea Ice Turbulence. *Geophysical Research Letters*,  
525 46(12), 6796–6803. Retrieved from [https://onlinelibrary.wiley.com/doi/](https://onlinelibrary.wiley.com/doi/abs/10.1029/2019GL082945)  
526 [abs/10.1029/2019GL082945](https://onlinelibrary.wiley.com/doi/abs/10.1029/2019GL082945) doi: 10.1029/2019GL082945
- 527 Wadhams, P., Squire, V. A., Goodman, D. J., Cowan, A. M., & Moore, S. C.  
528 (1988). The attenuation rates of ocean waves in the marginal ice zone. *Jour-*  
529 *nal of Geophysical Research: Oceans*, 93(C6), 6799–6818. Retrieved from  
530 <https://onlinelibrary.wiley.com/doi/abs/10.1029/JC093iC06p06799>  
531 doi: 10.1029/JC093iC06p06799

*JGR Oceans*

Supporting Information for

**Direct observations of wave-sea ice interactions in the Antarctic Marginal Ice Zone**

S. Wahlgren<sup>1</sup>, J. Thomson<sup>2</sup>, L. C. Biddle<sup>1,3</sup>, S. Swart<sup>1</sup>

<sup>1</sup> Department of Marine Sciences, University of Gothenburg, Gothenburg, Sweden

<sup>2</sup> Applied Physics Laboratory, University of Washington, Seattle, Washington

<sup>3</sup> Voice of the Ocean, Gothenburg, Sweden

**Contents of this file**

Figures S1 to S3

**Additional Supporting Information (Files uploaded separately)**

Captions for Videos S1 to S3

**Introduction**

The supporting information contains additional imagery of local sea ice condition. We provide photos taken from the ship during deployment and recovery of the SWIFT buoys, as well as time lapse videos with photos taken by the cameras mounted on the SWIFT buoys.



**Figure S1.** Photo of the sea ice taken from the research vessel during the deployment of SWIFT20 in austral spring (October 27 2019).



**Figure S2.** Photo of the sea ice taken from the research vessel during the deployment of SWIFT21 in austral spring (October 27 2019). The sea ice consisted of densely packed floes, and the buoy was deployed in the relatively open ship track.



**Figure S3.** Photo of the sea ice taken from the research vessel during the recovery of SWIFT21 in austral spring (November 8 2019).

**Video S1.** Time lapse of the on-board imagery captured by SWIFT21 during the winter deployment. Due to size restriction, only every 10<sup>th</sup> photo is shown. The full time lapse can be found here <https://doi.org/10.5281/zenodo.7845764>.

**Video S2.** Time lapse of the on-board imagery captured by SWIFT20 during the spring deployment. Due to size restriction, only every 10<sup>th</sup> photo is shown. The full time lapse can be found here <https://doi.org/10.5281/zenodo.7845764>.

**Video S3.** Time lapse of the on-board imagery captured by SWIFT21 during the spring deployment. Due to size restriction, only every 10<sup>th</sup> photo is shown. The full time lapse can be found here <https://doi.org/10.5281/zenodo.7845764>.